2022 44th Annual International Conference of
the IEEE Engineering in Medicine & Biology Society (EMBC)
Scottish Event Campus, Glasgow, UK, July 11-15, 2022

2022 44th Annual International Conference of the IEEE Engineering in Medicine & Biology Society (EMBC) | 978-1-7281-2782-8/22/$31.00 ©2022 IEEE | DOI: 10.1109/EMBC48229.2022.9871712

Contactless Heartbeat Measurement Using Speckle Vibrometry

Shuhao Que[1], Willem Verkruijsse[2], Mark van Gastel[2] and Sander Stuijk[1]

Abstract— **Monitoring of heart rate in patients in the general ward is necessary to assess the clinical situation of the patient. Currently, this is done via spot-checks on pulse rate manually or on heart rate using Electrocardiogram (ECG) by nurses. More frequent measurements would allow early detection of adverse cardiac events. In this work, we investigate a contactless measurement setup combined with a signal processing pipeline, which is based on speckle vibrometry (SV), to perform contactless heart rate monitoring of human subjects in a supine position, mimicking a resting scenario in the general ward. Our results demonstrate the feasibility of extracting heart rate with SV through varying textile thicknesses (i.e., 8 mm, 32 mm and 64 mm), with an error smaller than 3 beats per minute on average compared to the ground-truth heart rate derived from ECG.**

I. INTRODUCTION

In hospitalized patients, heart rate (or pulse rate) as one of the vital signs is measured to assess the clinical situation and possible deterioration of the patient [1] [2]. Currently, monitoring of heart rate in the general ward is done by nurses spot-checking pulse rate through pulse oximeter or heart rate through ECG every 4-6 hours [3]. Besides, according to a recent study [4], one-third of vital sign spot-checks are not done on time and one quarter are incomplete [2]. Such limited frequency might not be sufficient for early detection of adverse cardiac events since patients may experience deterioration between monitoring intervals [5] [2]. Thus, more frequent measurements are preferred. Current existing wearable devices have been proposed for continuous heart rate monitoring in the general ward, such as ViSi Mobile and HealthPatch [6]. Apart from ECG and pulse oximeter [2], other contact sensors also offer opportunity for general ward continuous heart rate monitoring, such as fabric-integrated multimode optical fiber [7] and finger plethysmography [8]. However, despite their wearable nature, these contact-based modalities still introduce inconvenience to patients' movement. Therefore, in this work, we investigate the feasibility of using speckle vibrometry (SV) as a contactless alternative for more frequent heart rate measurement.

SV technology can detect the motion-induced temporal variations of the laser speckle patterns [9]. A laser speckle pattern is essentially a random intensity distribution, produced when a coherent laser beam is reflected from a surface that is optically rough on the scale of the laser wavelength. Inside the speckle pattern, the granular spots of intensity that can be observed by using a defocused camera are called speckles. The speckle effect results from the interference among waves that share the same frequency but differ in phase and amplitude [10]. The laser speckle effect has long been investigated (e.g., estimation of ego-motion [11]) and SV has been used for various applications including speech [9] and heartbeat extraction [9] [12] [13]. SV enables magnification of micro-vibrations on the surface and therefore allows for heartbeat detection similar to Seismocardiogram (SCG) [14] and Gyrocardiogram (GCG) [15]. Other popular motion based remote sensing technologies include laser Doppler vibrometry (LDV) and radio frequency (RF). LDV can detect vibration velocity of the surface where the laser spot is focused, by comparing the frequency shift between the emitted and reflected laser beams [16]. Marchionni et al. [17] demonstrated the feasibility of non-contact monitoring of heart rate and respiration rate on preterm infants using LDV. Wang et al. [18] even managed to use pulsed laser vibrometer to monitor cardiac activity through clothes. RF can extract heartbeat by processing the phase variation information of the microwave radar signal [19]. Feasibility of heart rate extraction using RF has been demonstrated by [20] and [21]. Despite the contactless nature of LDV and RF for heartbeat monitoring, there are also downsides to consider. LDV can only detect the movement whose direction is along the incident laser beam [22] and the measured surface has to be reasonably reflective [23] [19] which often requires the use of retro-reflective materials on the skin [24] [25]. As for RF, the heartbeat-induced motion is very small compared to other detected motion, which renders isolation of the cardiac component difficult [26]. Furthermore, the positioning of the radar device and measuring distance is limited by limitations on power emission because of safety [26]. By comparison, SV does not require strict camera-surface positioning like LDV and no retro-reflective materials are needed since laser speckle patterns can be formed on any kind of optically rough surface (e.g., human skin and commonly used textiles). Besides, the use of a laser beam enables SV to measure at a further distance and be more precise and flexible in terms of region of interest selection.

Remote Photoplethysmography (PPG) [27] is another contactless sensing technology for heart rate monitoring, which is based on a camera to detect blood volume changes on the skin. In the general ward, textiles (e.g., bedsheet) are commonly used by patients. Remote PPG requires visible skin and textiles might pose a risk that it occludes the skin. Therefore, using ECG as reference, this work aimed at validating the feasibility of using SV for contactless heart

*This study was approved by the ethical review board of the Eindhoven University of Technology and funded by the NWO UMOSA project (17117).

[1]S. Que and S. Stuijk are with Eindhoven University of Technology, Eindhoven, The Netherlands. s.que@tue.nl; s.stuijk@tue.nl.

[2]M. van Gastel and W. Verkruijsse are with Philips Research, Eindhoven, The Netherlands. mark.van.gastel@philips.com; wim.verkruijsse@philips.com.

rate measurement through textiles while the subjects were lying on their back. We first conducted on-skin measurements on four selected anatomical locations (i.e., sternum, tricuspid, aortic and central abdomen) and selected tricuspid, which achieved the best performance with on average 0.3 beats of difference per minute compared with ECG, as the best aiming location for through-textile measurements. The obtained results showcase the feasibility of using SV to monitor heart rate at several spots on the skin including one that is relatively distant from the heart (i.e., central abdomen) and one spot (i.e., tricuspid area) through textiles.

II. Methods

A. SV and Motion Extraction

Our setup is based on a front-defocused camera system to register the motion of the imaged speckle pattern. Following the theoretical explanations presented by Zalevsky et al. in [9], when the camera is defocused, the imaging plane is shifted from the detected object to a plane positioned at a distance L_1 (see Figure 1) and L_2 is the distance between the camera focus plane and the camera lens. Under this imaging condition, neither transversal nor axial movement affects the distribution of the speckle pattern [9]. The tilt of the detected object manifests as displacements of the speckle pattern imaged in the camera, as presented by the following equation:

$$d = \frac{L_1 F}{L_2} \tan \alpha \tag{1}$$

where d denotes a relative shift of the speckle pattern due to object tilt, α denotes the tilt angle of the object and F denotes the focal length of the imaging lens. The shift of the speckle pattern is proportional to the amount of camera defocus (i.e. $\frac{L_1}{L_2}$) [28].

Video recordings of the laser speckle pattern were processed by a motion extraction algorithm to obtain heartbeat signals. In this work, we used the sub-pixel image registration algorithm proposed by Guizar-Sicairos et al. [29], where sub-pixel translations of the speckles along both x- and y-axes were obtained by first locating the cross-correlation peak using a coarse-to-fine up-sampling approach and then dividing the coordinates of the peak by the up-sampling factor. The values of L_1, L_2 and F in our experimental setup were about 0.6 m, 0.4 m, and 0.05 m respectively, under which condition, we selected the up-sampling factor as 100, which indicates a sub-pixel accuracy of 0.01 pixels

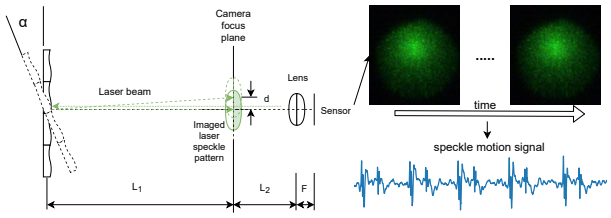

Fig. 1. Schematic of defocused camera system for speckle vibrometry.

that guarantees the detection of the minimum angular change represented as 0.00013 pixels/mm. The up-sampling factor of 100 was empirically selected to be sufficient to detect the motions induced by heartbeats.

B. Experimental Setup and Protocols

The experimental setup of SV for contactless heartbeat monitoring is shown in Figure 2. A monochrome camera with a 2.35 megapixel CMOS sensor (UI-3060CP-M-GL, IDS Imaging Development Systems GmbH) was used. An Aixiz Class-I green laser (AD-532-1-830) was mounted to a C-mount camera lens (M111FM50, Tamron) in parallel. The focus distance L_2 of the camera lens was set to the minimal value of 0.4 m (see Figure 2). The laser and camera view were along the z-axis. The distance between the camera and the bed surface was 125 cm, rendering the measuring distance approxmately 100 cm. For SCG/GCG signal acquisition, an inertial measurement unit (BWT901CL, WitMotion) was firmly attached to the subjects' sternum using double-sided skin tape (Nitto, ST-502-1). For the single-lead ECG signal acquisition, a Mind Media Nexus-10 was used with the BioTrace+ NX10 software package. This configuration was used in all experiments. Data from different devices was synchronized by introducing motion artifacts at the beginning of the measurements, yielding an estimated misalignment range from 0 ms to 150 ms.

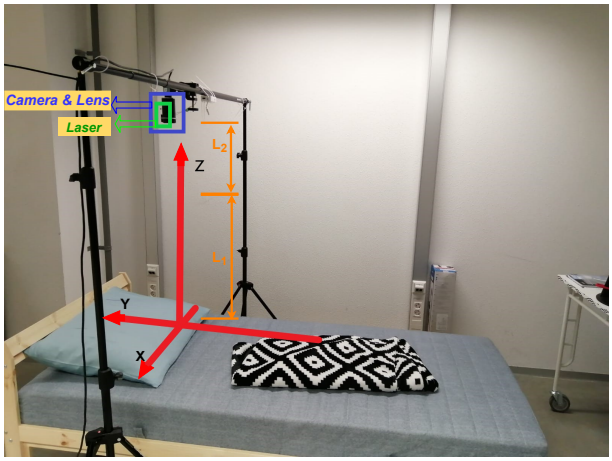

Fig. 2. Experimental setup for SV heart rate measurement. The blue rectangle indicates the positioning of the camera and the laser (in the green rectangle) is attached to the camera lens in an aligned fashion. The red arrows x and y indicate the x- and y-axes in the camera field of view, which also correspond to the two directions of the SV measurement.

The Ethical Review Board (ERB) of the Eindhoven University of Technology approved the data collection and processing protocol (ERB2020EE3) for this study. After obtaining their informed consent forms, a total of 9 healthy human subjects participated in the study (five males). Data collection was conducted on each subject while the subject was breathing spontaneously in a supine position. An indication of the selected anatomical locations is shown in Figure 3. The used textile materials are shown in Figure 4. The specifications of the devices used for the experiments

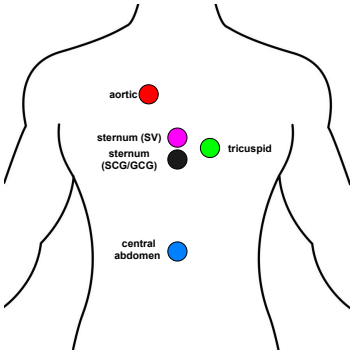

Fig. 3. Indication of the selected anatomical locations.

Fig. 4. Textile materials used for the study.

are presented in Table I. The detailed recording procedure for each subject is indicated in Table II. It is worth mentioning that the textiles were folded tightly and symmetrically once, once and three times to respectively obtain 2 layers of comforters, 2 layers of blankets and 3 layers of bedsheets. 8 and 16 layers of blankets were thus obtained by stacking 4 and 8 pieces of folded blankets respectively. 12 and 24 layers of bedsheets were thus obtained by stacking 4 and 8 pieces of folded bedsheets respectively. While each subject remained static in bed, the textiles were directly placed on them covering their whole upper torso without additional adjustment. For each separate recording, the textiles were removed and placed back on the subject.

C. Evaluation Metrics

Firstly, we proposed a method to derive a single measurement for SV. Secondly, using ECG as a reference, combined with two peak detection algorithms that are presented below, average heart rates (HR_a) were derived from the beat-to-beat intervals of the ECG and SV signals for comparison and quality assessment.

1) Derivation of SV measurement D_r: A SV signal has two directions, i.e., along its x- and y-axes. These are denoted as D_x and D_y (see Figure 2) in this work. By mapping the Cartesian coordinates to polar coordinates, we located the dominant heartbeat-induced vibration direction, denoted by $\hat{\theta}$, and thereby we derived a single measurement for SV denoted by D_r, which is independent of the camera-surface orientation. The conversion equation is presented below:

$$D_r = D_x \cdot cos\hat{\theta} + D_y \cdot sin\hat{\theta} \tag{2}$$

For each one-minute recording of SV measurements, to locate one polar angle value that represents the dominant vibration direction of the heartbeat induced peaks, the amplitudes calculated by $\sqrt{D_x^2 + D_y^2}$ were derived in four Cartesian quadrants respectively. The Cartesian quadrant with the highest 90th percentile values of the amplitudes were selected and the dominant vibration angle was the median of all existing θ values within this plane, denoted by $\hat{\theta}$. The derivation of $\hat{\theta}$ is presented below:

$$\begin{cases} C = \text{argmax}_{C_j}\{P_{90}(\sqrt{D_x^2 + D_y^2})_{[(x,y)\in C_j]}\}, & C_j \text{ = j-th Cartesian quadrant} \\ \theta_i = \arctan\frac{D_{y_i}[(x_i,y_i)\in C]}{D_{x_i}[(x_i,y_i)\in C]} & \text{i = 1,2,3,...,N} \\ \hat{\theta} = M(\{\theta_i\}) \end{cases} \tag{3}$$

where M denotes the median and N denotes the number of x- and y-coordinate pairs of the whole recording in the selected Cartesian quadrant C.

The same procedure was applied to x- and y-axes of GCG to obtain G_r for a fair waveform comparison with D_r. However, x- and y-axes of SCG appeared to be too noisy so only the z-axis A_z was used for waveform comparison.

2) Peak detection: To detect the peaks in the SCG, GCG and SV signals, we propose the following algorithm consisting of three steps. Steps 1 and 2 were adopted from Tadi et al. [30]:

- **Step 1**: the signal was first passed through a fourth-order Butterworth IIR high-pass filter with a cutoff frequency equal to 0.5 Hz, with the purpose of removing baseline wander and respiratory components. The Hilbert transform was applied to the high-pass filtered signal to obtain its analytic signal. Since Hilbert transform yields a 90° phase shift, the magnitude of the analytic signal was computed to derive the Hilbert amplitude envelope.

- **Step 2**: the computed Hilbert amplitude envelope was then passed through a third-order Butterworth IIR band-pass filter with cutoff frequencies of 0.5 Hz and 3 Hz to obtain a simpler structured waveform that contains the same periodicity as the original signal, named as the filtered Hilbert envelope signal. Although the participants were all healthy with a normal resting heart rate range (60-100 beats per minute), the lower bound 0.5 Hz (i.e., 30 beats per minute) and the upper bound 3 Hz (i.e., 180 beats per minute) were chosen since in the general ward patients might exhibit abnormal heart rates.

- **Step 3**: we employed the find_peaks[1] function from the Scipy library of Python to perform peak detection on the filtered Hilbert envelope signal with the required minimal peak height set as 0. The envelope peaks, i.e., the detected peak locations of the filtered Hilbert envelope signal, were then mapped back to the original

[1]https://docs.scipy.org/doc/scipy/reference/generated/scipy.signal.find_peaks.html

TABLE I

DEVICE SPECIFICATIONS

Camera & Lens		**Laser**		**Accelerometer**		**ECG**		**Positioning of camera & laser**	
Frame rate (fps)	360	Wavelength (nm)	532	Fs (Hz)	200	Fs (Hz)	256	Elevation (degrees)	90
Exposure (ms)	2.002	Power (mW)	$\leq$1	Acc (g)	$\pm$2	Nr. of leads	1	Distance (cm)	100
Resolution (pixels)	280×330			Gyr (degree/s)	$\pm$250				
Aperture (f-stop)	F/1.8								
Focus dist. L_2 (m)	0.4								

TABLE II

RECORDING PROCEDURE ON EACH SUBJECT

Anatomical location	**Textile material**	**Layer thickness**	**Number of layers**	**Duration of one recording**	**Repetitions per subject**	**Number of subjects**
Sternum	N/A	0 mm	0	1 minute	3	9
Tricuspid	N/A	0 mm	0	1 minute	3	9
Aortic	N/A	0 mm	0	1 minute	3	9
Central abdomen	N/A	0 mm	0	1 minute	3	9
Tricuspid	N/A	0 mm	0	1 minute	3	9
Tricuspid area	Furry blanket	8 mm	2	1 minute	3	9
Tricuspid area	Furry blanket	32 mm	8	1 minute	3	9
Tricuspid area	Furry blanket	64 mm	16	1 minute	3	9
Tricuspid area	Cotton sheet	8 mm	3	1 minute	3	9
Tricuspid area	Cotton sheet	32 mm	12	1 minute	3	9
Tricuspid area	Cotton sheet	64 mm	24	1 minute	3	9
Tricuspid area	Cotton comforter	32 mm	1	1 minute	3	9
Tricuspid area	Cotton comforter	64 mm	2	1 minute	3	9

signal to locate the original peak locations through window-searching of local maximal amplitudes. The range of the i-th window was defined as $[0.5*(peak_i - peak_{i-1}),\ peak_i+A]$, where A was empirically selected to be 150 ms to avoid locating the peak of the next cardiac cycle.

As for the R-peak detection of ECG signals, the implementation of the widely adopted algorithm proposed by W. Engelse and C. Zeelenberg [31] with the modifications proposed by A. Lourenco et al. [32] was used, which proved to be capable of correctly detecting noisy single heartbeats [32].

3) Average absolute heart rate errors: Using ECG as reference, the average absolute heart rate error (AHRE_a) of each subject's three repeated measurements can be calculated from the following equation:

$$AHRE_a = \frac{\sum_{i=1}^{3} |HR_a(ECG_i) - HR_a(SV_i)|}{3} \quad (4)$$

4) Average peak amplitude of D_r: By employing the peak detection algorithm mentioned above, both the maximal positive and negative amplitudes of SV measurements were determined within each search window formulated in Step 3. The average peak amplitude was thus derived from the average of three repeated measurements from each subject.

III. RESULTS AND DISCUSSIONS

A. Waveform of SV Measurement

Since both GCG and SCG signals were obtained from the sternum, we chose SV measurements D_r collected from the sternum for comparison, along with ECG. Figure 5 displays the ensemble peaks from these four measurements collected from two subjects which show clear raw waveforms. ECG demonstrates the most stable peak morphology among all. In the upper plot (i.e., subject 5), the peak morphology of SV measurement D_r is most similar to that of GCG measurement G_r, both exhibiting low variability. In the lower plot (i.e., subject 2), the peak morphology of D_r is also most similar to that of G_r, both exhibiting larger variability.

For through-textile measurement, Figure 6 shows 10-second segments from subject 2 with respect to different textile materials and layer thicknesses. Subject 2 was selected because the collected measurements in all textile coverage scenarios exhibited clear raw waveforms. It can be observed that textile layers dampened the amplitudes of SV measurements. Figure 7 further shows that for most subjects, regardless of the textile materials, textile layers have dampening effect on the amplitudes of SV measurements in general. Exceptions are with 8 mm of bedsheet (subjects 4, 7, and 8). We speculate that 8 mm of bedsheet can enhance high-frequency heartbeat motions and dampen low-frequency respiratory ones in certain cases, which are probably dependent on body mass index (BMI), respiration-to-heartbeat magnitude ratio etc. and require further investigation.

B. Feasibility of SV Heart Rate Measurement

Figure 8 illustrates the distributions of AHRE_a between ECG and on-skin SV signals calculated from all 9 subjects. It can be observed that for all anatomical locations, the median AHRE_a are less than 1 BPM with the largest deviation less than 3 BPM, indicating the feasibility of using SV to monitor heart rate on uncovered skin. SV signal on both tricuspid and aortic yielded the lowest AHRE_a while central abdomen the highest, but these differences were not significant. Figure 9

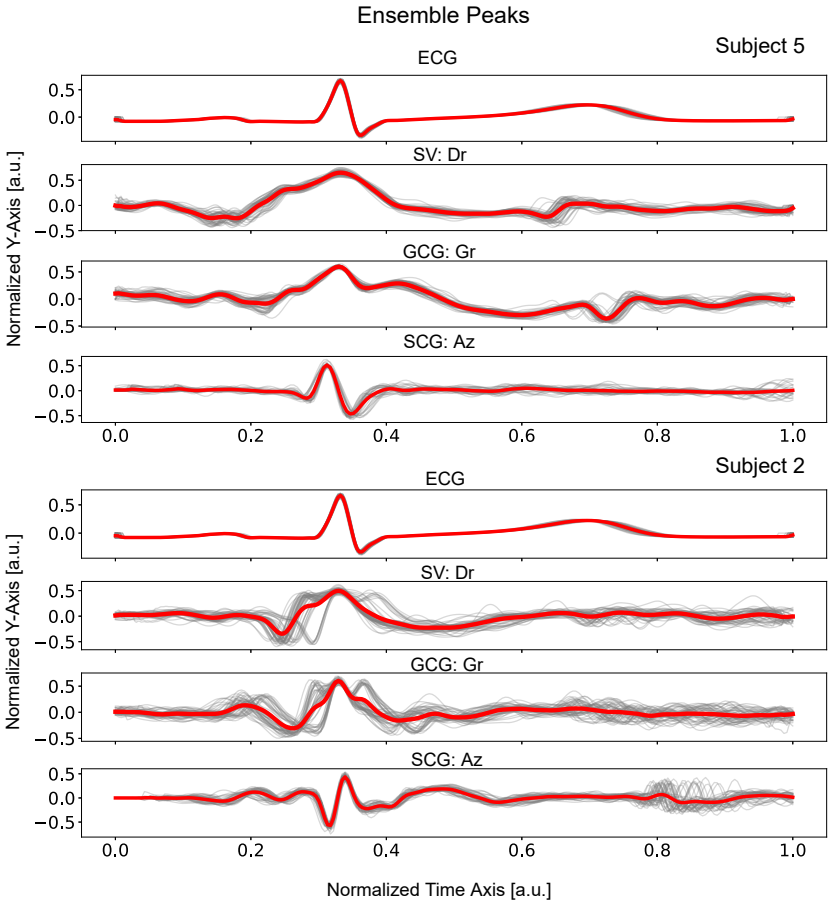

Fig. 5. Ensemble peaks of ECG, on-sternum SV, GCG and SCG from subjects 5 and 2. The corresponding measurements were synchronised based on motion artifacts with peak misalignment less than 150 ms. Each graph is composed by 50 segments sampled from one continuous measurement.

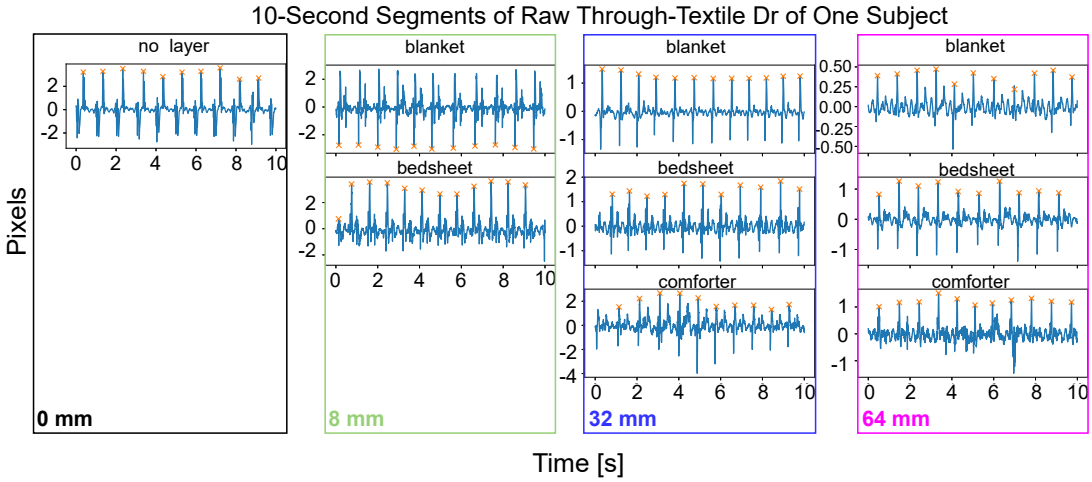

Fig. 6. 10-second segments of raw D_r of subject 2. The proposed peak detection algorithm was applied to all these segments. The y-axis of each individual plot denotes pixels and the x-axis denotes time in seconds.

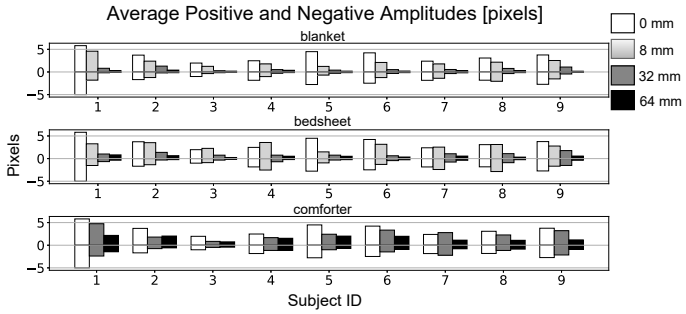

Fig. 7. Average amplitudes of the positive and negative peaks in the raw waveform of D_r from all 9 subjects.

demonstrates that for the four anatomical locations, despite the difference in body shape between the two genders around the chest area, no significant differences were found in the distributions of AHRE_a. If we combine the four anatomical locations, as shown in Figure 10, still no statistically signifcant difference was found between two genders (p-value=0.126). At each anatomical location, there is one male subject that exhibits higher AHRE_a values. We speculate that it was because of the subject's BMI (>25), which might have negative impact on heart rate estimation based on SV.

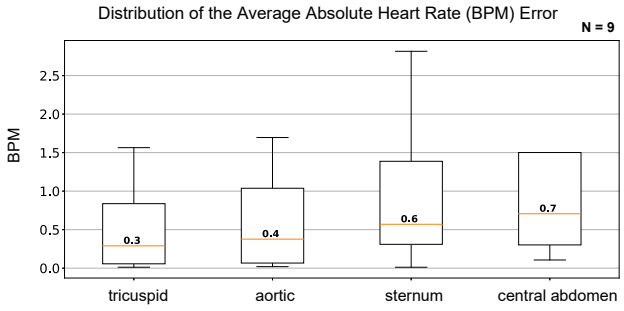

Fig. 8. Average absolute heart rate error (BPM) of on-skin heartbeat measurement. The number of data points for each anatomical location is 9 (i.e., N = 9), composed by the average results of 3 repetitions from all 9 subjects. No statistical significance was found among these distributions according to Kruskal-Wallis H test [33].

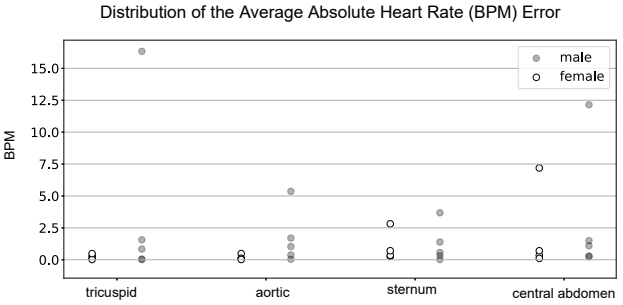

Fig. 9. Average absolute heart rate error (BPM) of on-skin heartbeat measurement: comparison between males and females. The numbers of data points for each anatomical location are 4 and 5 for females and males respectively. No statistical significance was found according to Kruskal-Wallis H test.

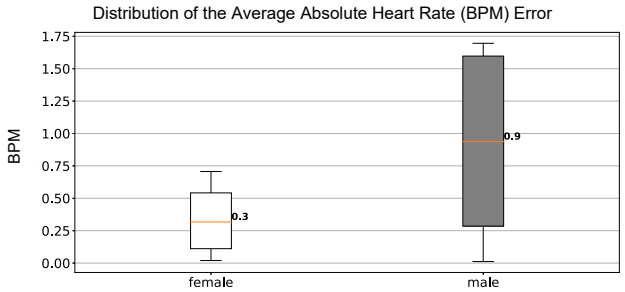

Fig. 10. Average absolute heart rate error (BPM) of on-skin heartbeat measurement: comparison between males and females. The numbers of data points for each anatomical location are 16 and 20 for females and males respectively. No statistical significance was found according to Kruskal-Wallis H test (p-value=0.126).

Figure 11 illustrates that compared with on-skin SV, all three textile materials did not introduce significant differences with 8 mm or 32 mm of layer thickness. However, when the layer thickness was 64 mm, bedsheet layers yieled slight increase in both median AHRE_a and interquartile range (IQR) values (p-value=0.031). Both comforter and blanket layers yielded significant increases (p-value=0.031, p-value=0.012). Therefore, it can be concluded that SV can provide accurate heart rate measurements even through 64 mm of bedsheets with median AHRE_a less than 2 BPM, which should suffice for through-textile measurement in the general ward. However, if the textile material was a blanket or a comforter, SV was less accurate when the layers have a thickness of 64 mm and exhibited larger values of both median AHRE_a (i.e., more than 2 BPM) and IQR, where blanket layers yielded the worst performance. The blanket material used in the experiments was the softest, which potentially made it more predisposed to relative displacements between the skin surface and the textiles and that could hinder the propagation of vibration from the heart to the textile layer surface.

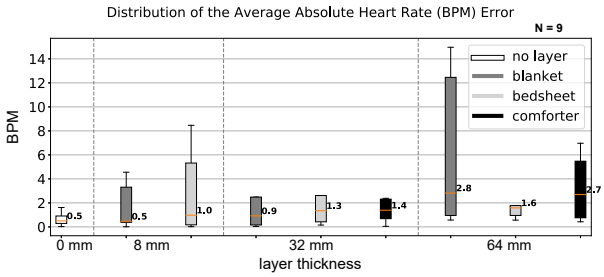

Fig. 11. Average absolute heart rate errors (BPM) of through-textile heartbeat measurement. The number of data points for each textile coverage scenario is 9 (i.e., N = 9), composed by the average results of 3 repetitions from all 9 subjects. According to Kruskal-Wallis H test, statistical significance was found between 0 mm and 64 mm (blanket: p-value=0.012; bedsheet: p-value=0.031; comforter: p-value=0.031).

IV. Conclusion

With proper on-skin selection of anatomical locations, SV is able to provide accurate heartbeat measurements through

textiles within 3 BPM error on average, serving as a contactless alternative to ECG in the general ward. Our current study is limited to the supine resting position and the anatomical location is limited to tricuspid area in case of through-textile measurement. Therefore, future work needs to investigate if SV still works when the resting position is lateral and if other anatomical locations that are relatively distant from the heart (e.g., central abdomen) can also provide through-textile heartbeat measurement. Subjects were asked to remain still during recording, where motion distortions that can happen in the general ward were not taken into consideration. The magnitude and frequency of respiratory motions both have impact on the quality of the extracted heartbeat-induced motions from SV videos, which is not addressed in this work due to lack of breathing belts that can quantify such effects. Future work needs to look into the detection and cancellation of motion distortions that can be present in the general ward. The effects of respiratory motions and BMI on SV measurements should also be addressed and quantified.

ACKNOWLEDGMENT

Special thanks to Wenjin Wang and Xi Long.

REFERENCES

[1] Elliott, M. and Coventry, A., 2012. Critical care: the eight vital signs of patient monitoring. British Journal of Nursing, 21(10), pp.621-625.

[2] Michard, F. and Kalkman, C.J., 2021. Rethinking Patient Surveillance on Hospital Wards. Anesthesiology.

[3] Michard, F., Bellomo, R. and Taenzer, A., 2019. The rise of ward monitoring: opportunities and challenges for critical care specialists. Intensive care medicine, 45(5), pp.671-673.

[4] Eddahchouri, Y., Koeneman, M., Plokker, M., Brouwer, E., van de Belt, T.H., van Goor, H. and Bredie, S.J., 2021. Low compliance to a vital sign safety protocol on general hospital wards: a retrospective cohort study. International Journal of Nursing Studies, 115, p.103849.

[5] Hands, C., Reid, E., Meredith, P., Smith, G.B., Prytherch, D.R., Schmidt, P.E. and Featherstone, P.I., 2013. Patterns in the recording of vital signs and early warning scores: compliance with a clinical escalation protocol. BMJ quality & safety, 22(9), pp.719-726.

[6] Weenk, M., Bredie, S.J., Koeneman, M., Hesselink, G., van Goor, H. and van de Belt, T.H., 2020. Continuous monitoring of vital signs in the general ward using wearable devices: randomized controlled trial. Journal of medical Internet research, 22(6), p.e15471.

[7] Bennett, A., Beiderman, Y., Agdarov, S., Beiderman, Y., Hendel, R., Straussman, B. and Zalevsky, Z., 2020. Monitoring of vital bio-signs by analysis of speckle patterns in a fabric-integrated multimode optical fiber sensor. Optics Express, 28(14), pp.20830-20844.

[8] Pant, S., Umesh, S. and Asokan, S., 2020. A novel approach to acquire the arterial pulse by finger plethysmography using fiber Bragg grating sensor. IEEE Sensors Journal, 20(11), pp.5921-5928.

[9] Zalevsky, Z., Beiderman, Y., Margalit, I., Gingold, S., Teicher, M., Mico, V. and Garcia, J., 2009. Simultaneous remote extraction of multiple speech sources and heart beats from secondary speckles pattern. Optics express, 17(24), pp.21566-21580.

[10] Dainty, J.C. ed., 2013. Laser speckle and related phenomena (Vol. 9). Springer science & business Media.

[11] Jo, K., Gupta, M. and Nayar, S.K., 2015. Spedo: 6 dof ego-motion sensor using speckle defocus imaging. In Proceedings of the IEEE International Conference on Computer Vision (pp. 4319-4327).

[12] Ozana, N., Margalith, I., Beiderman, Y., Kunin, M., Campino, G.A., Gerasi, R., Garcia, J., Mico, V. and Zalevsky, Z., 2015. Demonstration of a remote optical measurement configuration that correlates with breathing, heart rate, pulse pressure, blood coagulation, and blood oxygenation. Proceedings of the IEEE, 103(2), pp.248-262.

[13] Havakuk, O., Sadeh, B., Merdler, I., Zalevsky, Z., Garcia-Monreal, J., Polani, S. and Arbel, Y., 2021. Validation of a novel contact-free heart and respiratory rate monitor. Journal of Medical Engineering & Technology, pp.1-9.

[14] Zanetti, J.M. and Salerno, D.M., 1991, January. Seismocardiography: a technique for recording precordial acceleration. In Computer-Based Medical Systems-Proceedings of the Fourth Annual IEEE Symposium (pp. 4-5). IEEE Computer Society.

[15] Tadi, M.J., Lehtonen, E., Saraste, A., Tuominen, J., Koskinen, J., Teräs, M., Airaksinen, J., Pänkäälä, M. and Koivisto, T., 2017. Gyrocardiography: A new non-invasive monitoring method for the assessment of cardiac mechanics and the estimation of hemodynamic variables. Scientific reports, 7(1), pp.1-11.

[16] Kon, S., Oldham, K. and Horowitz, R., 2007, April. Piezoresistive and piezoelectric MEMS strain sensors for vibration detection. In Sensors and Smart Structures Technologies for Civil, Mechanical, and Aerospace Systems 2007 (Vol. 6529, p. 65292V). International Society for Optics and Photonics.

[17] Marchionni, P., Scalise, L., Ercoli, I. and Tomasini, E.P., 2013. An optical measurement method for the simultaneous assessment of respiration and heart rates in preterm infants. Review of Scientific Instruments, 84(12), p.121705.

[18] Wang, C.C., Trivedi, S., Kutcher, S., Rodriguez, P., Jin, F., Swaminathan, V., Walters, F. and Prasad, N.S., 2014. Non-Contact Cardiac Activity Monitoring using Pulsed Laser Vibrometer. Sensors & Transducers, 162(1), p.173.

[19] Taebi, A., Solar, B.E., Bomar, A.J., Sandler, R.H. and Mansy, H.A., 2019. Recent advances in seismocardiography. Vibration, 2(1), pp.64-86.

[20] Kuo, H.C., Chou, C.C., Lin, C.C., Yu, C.H., Huang, T.H. and Chuang, H.R., 2015, May. A 60-GHz CMOS direct-conversion Doppler radar RF sensor with clutter canceller for single-antenna noncontact human vital-signs detection. In 2015 IEEE Radio Frequency Integrated Circuits Symposium (RFIC) (pp. 35-38). IEEE.

[21] Sacco, G., Piuzzi, E., Pittella, E. and Pisa, S., 2020. An FMCW radar for localization and vital signs measurement for different chest orientations. Sensors, 20(12), p.3489.

[22] Scalise, L., Marchionni, P. and Ercoli, I., 2010, April. Optical method for measurement of respiration rate. In 2010 IEEE International Workshop on Medical Measurements and Applications (pp. 19-22). IEEE.

[23] Taebi, A., 2018. Characterization, classification, and genesis of seismocardiographic signals.

[24] Campo, A., Segers, P., Heuten, H., Goovaerts, I., Ennekens, G., Vrints, C., Baets, R. and Dirckx, J., 2014. Non-invasive technique for assessment of vascular wall stiffness using laser Doppler vibrometry. Measurement Science and Technology, 25(6), p.065701.

[25] Li, Y., Segers, P., Dirckx, J. and Baets, R., 2013. On-chip laser Doppler vibrometer for arterial pulse wave velocity measurement. Biomedical optics express, 4(7), pp.1229-1235.

[26] Kebe, M., Gadhafi, R., Mohammad, B., Sanduleanu, M., Saleh, H. and Al-Qutayri, M., 2020. Human vital signs detection methods and potential using radars: A review. Sensors, 20(5), p.1454.

[27] van Gastel, M., Stuijk, S. and de Haan, G., 2015. Motion robust remote-PPG in infrared. IEEE Transactions on Biomedical Engineering, 62(5), pp.1425-1433.

[28] Wu, N. and Haruyama, S., 2019, May. Real-time sound detection and regeneration based on optical flow algorithm of laser speckle images. In 2019 28th Wireless and Optical Communications Conference (WOCC) (pp. 1-4). IEEE.

[29] Guizar-Sicairos, M., Thurman, S.T. and Fienup, J.R., 2008. Efficient subpixel image registration algorithms. Optics letters, 33(2), pp.156-158.

[30] Tadi, M.J., Lehtonen, E., Hurnanen, T., Koskinen, J., Eriksson, J., Pänkäälä, M., Teräs, M. and Koivisto, T., 2016. A real-time approach for heart rate monitoring using a Hilbert transform in seismocardiograms. Physiological measurement, 37(11), p.1885.

[31] Engelse, W.A. and Zeelenberg, C., 1979. A single scan algorithm for QRS-detection and feature extraction. Computers in cardiology, 6(1979), pp.37-42.

[32] Lourenço, A., Silva, H., Leite, P., Lourenço, R. and Fred, A.L., 2012, February. Real Time Electrocardiogram Segmentation for Finger based ECG Biometrics. In Biosignals (pp. 49-54).

[33] Kruskal, W.H. and Wallis, W.A., 1952. Use of ranks in one-criterion variance analysis. Journal of the American statistical Association, 47(260), pp.583-621.